PHYSICAL REVIEW E, VOLUME 65, 020301(R)

# Particle motion in gas-fluidized granular systems by pulsed-field gradient nuclear magnetic resonance

Ralf Savelsberg, Dan E. Demco, Bernhard Blümich, and Siegfried Stapf
*Lehrstuhl für Makromolekulare Chemie, ITMC, RWTH Aachen, Worringerweg 1, D-52074 Aachen, Germany*
(Received 13 August 2001; published 16 January 2002)

Nuclear magnetic resonance *k*-space and *q*-space imaging methods were applied for the first time to monitor the time-averaged density variations and the random motion of granular particles in the presence of gas flow of variable velocity in a model gas-fluidized bed reactor. The transitions toward fluidization, bubbling phase, and slugging phase are visible as sudden changes in the density and the root mean-squared displacement. The onset of these transitions is shown to depend on the particle sizes for a given cell geometry. The effective diffusion coefficients are measured and the distributions of particle displacements, or propagators, are presented.

DOI: 10.1103/PhysRevE.65.020301 PACS number(s): 45.70.−n, 47.55.Kf, 83.85.Fg, 05.60.−k

The dynamics of granular media has recently attracted considerable interest particularly from the viewpoint of comparisons to ''classical'' physical states such as liquids and gases. In granular media, macroscopic particles take over the place of molecules and the main difference to classical states of matter lies in the fact that, due to energy dissipation occurring because of particle collisions, the equivalents to phase transitions are brought about by a permanent influx of energy. A particularly interesting case of a granular medium is the gas-fluidized bed in which energy is provided by a continuous gas flow from the bottom of a vessel filled with macroscopic particles. This model is of further importance because it represents the geometry for a wide range of industrial processes such as catalysis of gas-phase reactions and transports of powders [1,2]. Such a vessel contains typically upwards from $10^4$ particles and thus provides a sufficient number for statistical averaging, while numerical simulations for similar numbers remain feasible. In recent work, such numerical simulations have been performed [3,4] and a variety of phenomena, including bubbling and slugging phases as well as apparent phase transitions, were described in terms of particle volume fraction oscillations and velocity distributions. However, direct experimental evidence for the dynamical properties of gas-fluidized beds is difficult to achieve, one recent approach reported in the literature being the use of diffusing-wave spectroscopy (DWS) in systems of transparent glass particles which was sensible to particle displacements of $10^{-6}$ m or less [5,6], but could not distinguish between displacements in different directions.

A much more direct approach is provided by techniques derived from nuclear magnetic resonance (NMR) imaging [7,8] with displacements from about $10^{-6}$ m being accessible, thus, in principle, representing a method complementary to DWS. Applications of nuclear magnetic resonance techniques to investigate the dynamics of granular media under rotating [9] and vibrating boundary conditions [10] have been presented recently. The idea on which NMR imaging is based lies in a spatial encoding of particle positions. If the magnetic field consists of a homogeneous contribution $\boldsymbol{B_0}=(0,0,B_0)^t$ and a spatially constant gradient $\boldsymbol{G}=(\partial B_z/\partial x,\ \partial B_z/\partial y,\ \partial B_z/\partial z)^t$, the Larmor precession frequency of a spin species of gyromagnetic ratio $\gamma$ is then given by

$$\omega(\boldsymbol{r})=-\gamma(|\boldsymbol{B_0}|+\boldsymbol{G}\cdot\boldsymbol{r}) \tag{1}$$

and thus depends linearly on the position of the spins in the direction of the applied gradient $\boldsymbol{G}$. The Fourier transform of the signal directly gives a one-dimensional distribution of spin densities, or a profile of the sample. Likewise, a short gradient pulse of duration $\delta$ leads to an accumulation of a phase shift $\phi(\boldsymbol{r})=\gamma\delta\boldsymbol{G}\cdot\boldsymbol{r}$ which correlates the position of spins with the phase of their resonance signal.

While frequency encoding or phase encoding represent the means to produce images of samples containing NMR-sensitive spins (in most cases protons), a twofold phase encoding, employing a gradient pair with equal but opposite effective amplitude $\boldsymbol{G}$ separated by a time interval $\Delta$, is sensitive to particle *displacements* during this interval. The normalized signal amplitude as a function of gradient strength for such a double-encoding experiment can be written as [7]

$$\tilde{S}(\boldsymbol{q},\Delta)=S(\boldsymbol{q},\Delta)/S(0,\Delta)=\int \overline{P}(\boldsymbol{R},\Delta)\exp[i2\pi\boldsymbol{q}\cdot\boldsymbol{R}(\Delta)]d\boldsymbol{R}, \tag{2}$$

where $\boldsymbol{q}=(2\pi)^{-1}\gamma\delta\boldsymbol{G}$, the Fourier conjugate variable to displacement $\boldsymbol{R}$, is the equivalent to the wave number in scattering experiments and has the dimension of reciprocal length. The distribution of particle displacements during $\Delta$, or average propagator, $\overline{P}(\boldsymbol{R},\Delta)$, can thus directly be obtained by Fourier transformation of the $\boldsymbol{q}$-space data. Note that this relation is strictly true only if $\delta\ll\Delta$.

From the propagator, moments of displacements can be computed; for random motion without net material transport, the first nonvanishing moment is the mean-squared displacement which can be expressed as $\langle\boldsymbol{R}^2\rangle=6D(\Delta)\Delta$, where the proportionality constant $D(\Delta)$ is the dispersion coefficient for material transport in the system. The time dependence of $D(\Delta)$ is related to the velocity autocorrelation function (VACF) by [9]

$$D(\Delta)=\int_0^\Delta\left(1-\frac{\tau}{\Delta}\right)\langle v(0)v(\tau)\rangle d\tau \tag{3}$$

for stochastic systems at equilibrium, where the VACF depends on the time *differences* only. In ordinary liquids and

 

gases, collision times are usually short compared to the timescale of NMR diffusion measurements, so that a time-independent asymptotic value $D=\lim_{\Delta\to\infty}D(\Delta)$ is observed. For granular particles, on the other hand, the time dependence of $D(\Delta)$ has to be taken into account.

Rather than computing $D(\Delta)$ from the propagator $\overline{P}(\boldsymbol{R},\Delta)$, it is also possible to obtain it more directly from the initial slope of the signal function $\tilde{S}(q,\Delta)$ in a one-dimensional (1D) NMR experiment [11]

$$D(\Delta)\approx-(4\pi^2\Delta)^{-1}\lim_{q\to0}\frac{\partial\ln|\tilde{S}(q,\Delta)|}{\partial q^2}. \tag{4}$$

The representation of the experimental data in $\boldsymbol{q}$ space has one further advantage. It was shown that structural features of a medium in which restricted diffusion takes place lead to the occurrence of peaks or shoulders at the reciprocal values of these lengths. For example, diffusion of liquids in packings of monodisperse spherical beads show such diffraction-like phenomena at the reciprocal of the bead diameter [12,13]. The signal function $\tilde{S}(q,\Delta)$ can thus be exploited as a means to estimate such restriction sizes.

In this paper, we present NMR imaging and diffusion experiments on a gas-fluidized bed consisting of a 21 mm inner-diameter glass vessel oriented vertically and parallel to the direction of the magnetic-field $\boldsymbol{B_0}$, which at its bottom was connected to a pipe supplying a continuous flow of dry air. In the vessel, the granular medium was supported by a glass frit which also served as a gas diffusor. As granular particles, we have chosen poppy seeds (diameter 500–800 $\mu$m) and sieved catalyst particles (type G-43, Süd-Chemie, Germany) in three different grain size ranges, 200–250, 140–200, and 112–140 $\mu$m, respectively, the filling height being 30 mm. The NMR proton signal came from the oil component of the seeds and from acetone adsorbed into the catalyst particles, respectively. Acetone was filled into the catalyst material until full saturation of the pore volume (0.39 $cm^3/g$) was achieved. Due to evaporation from the particles, a loss of approximately 20% of the acetone after six hours was observed. All experiments had thus been restricted to total durations of less than three hours.

The profiles along the vertical direction were obtained by single-point imaging, where the signal intensity was acquired following a low flip-angle rf pulse in the presence of a magnetic-field gradient which was varied in 128 steps. Using this method, the disturbing effect of particle motion was minimized due to the short acquisition time of approximately 10 $\mu$s which led to a considerable improvement of the image quality compared to the conventional frequency encoding technique.

The spin density near the central region of the granular bed was measured from the 1D $z$ profiles ($z$ axis parallel with the cell axis) and normalized to their value in the absence of gas flow. The superficial air velocity, defined by the ratio of volume flow rate and total cross section of the sample cylinder, is used as a parameter. In Fig. 1(a), this normalized density reflects the different stages in the dynamic behavior of the gas-fluidized bed: at 20 cm/s for

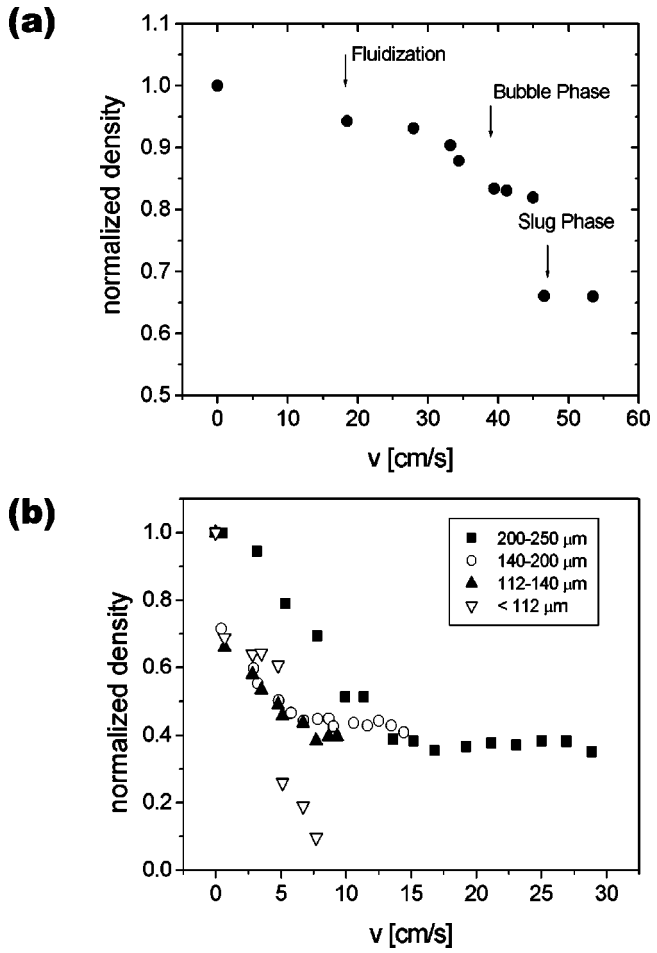


FIG. 1. Densities of gas-fluidized beds for different particle sizes, normalized by the density at zero flow rate. Data are plotted as a function of the superficial gas velocity. (a) Poppy seeds; (b) catalyst particles of different diameter ranges.

poppy seeds, fluidization has occurred; at 35 cm/s, a further decrease of the density indicates the formation of bubbles, while around 45 cm/s, the bubble size becomes equal to the bed cross section and the slugging phase starts to occur, with particle ejection following at even larger flow rates. The main difference observed for the smaller catalyst particles [see Fig. 1(b)] lies in the fact that bubbling occurs at a considerably larger expansion of the bed. Before the onset of bubbling, the density decreases monotonously. Due to a higher influence of cohesive forces, the beds containing the smallest particles are most difficult to fluidize, and bubbling and slugging occur at small air flow rates. These observations are in good agreement with results previously reported in [6] for a smaller range of flow rates but similar particle sizes.

We have investigated the translational behavior of fluidized particles in the direction of the air stream by NMR $\boldsymbol{q}$-space imaging, using $\delta=0.4$ ms and an encoding time $\Delta$ of 1.4 ms. All experiments describe a statistical average over the whole bed as well as a time average over typically one hour for a given gas flow rate. In Fig. 2(a), the signal function $\tilde{S}(q)$ is shown for catalyst particles of 200–250 $\mu$m diameter as a function of the air velocity. In general, a sharp

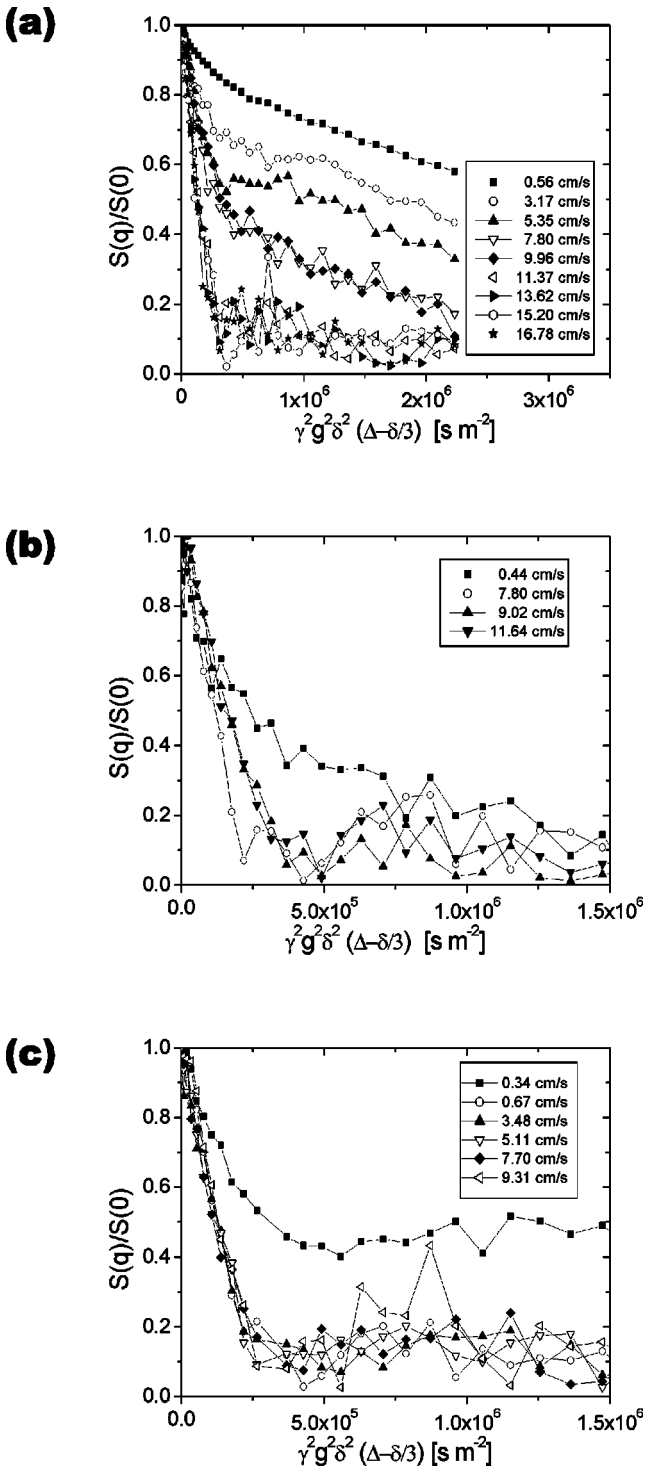


FIG. 2. Normalized signal intensity $S(\boldsymbol{q})/S(0)$ for different particle sizes and air flow velocities. (a) Particle size 200–250 $\mu$m; (b) 140–200 $\mu$m; (c) 112–140 $\mu$m.

decrease is followed by a more slowly decaying function. The average diffusion coefficient was computed from the initial slope according to Eq. (4) and is presented in Fig. 3. For $v<10$ cm/s, it is possible to fit a biexponentially decaying function. The fast component increases up to about $1.5\times10^{-6}$ m$^2$/s, while the slowly increasing second component of approximately $10^{-7}$ m$^2$/s is found with a reduced

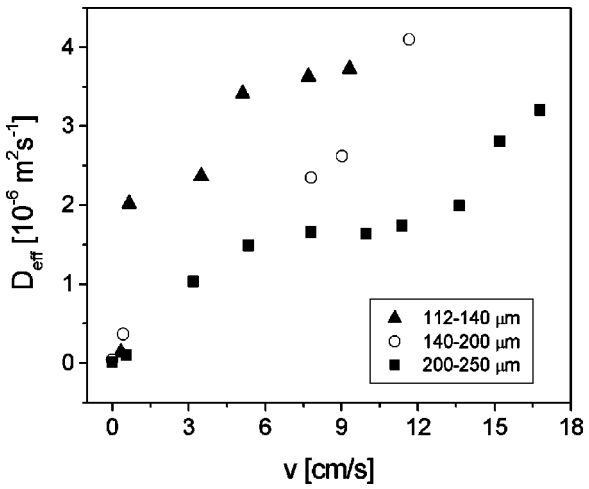


FIG. 3. Effective self-diffusion coefficient for beds of catalyst particles of different sizes obtained by Eq. (4).

relative weight at growing air flow rates. In this range, bubbling does not yet occur, but the relative bed density $\rho_{rel}$ is reduced from 1 to 0.5.

In order to understand this behavior, one can tentatively assume that the bed density reduction is equivalent to an introduction of homogeneously distributed ''free volume'' around each particle of radius $r_0$. This allows free oscillations of $\pm r_0(\rho_{rel}^{-1/3}-1)$ in each spatial direction. One would expect oscillation amplitudes up to 30 $\mu$m which correspond to an upper bound of the effective diffusion coefficient of $D(\Delta)=(30\ \mu\text{m})^2/2\Delta\approx3\times10^{-7}$ m$^2$/s. In reality, the mean-squared displacement is expected to be considerably smaller than this maximum value, leading to a value of $D$ which is in agreement with the slow component of the experimental data. Moreover, if the maximum particle velocity is set to the gas velocity $v$, then the average time between two particle collisions can be estimated as $\tau_c=r_0(\rho_{rel}^{-1/3}-1)/v$. For the measured velocities, one obtains $\tau_c$ of less than 300 $\mu$s, thus each particle is expected to encounter many collisions during the experimental encoding time $\Delta$ of 1.4 ms. The approximation of particle motion as a case of restricted diffusion inside a cage of surrounding particles therefore seems reasonable. The fast diffusion component, on the other hand, corresponds to a large-scale, coherent motion process in the bed which is not hindered by particle collisions. This result is at variance to the findings in [6] where for particles of similar size, a short-time ballistic regime ($\Delta\ll\tau_c$) is followed by a very slow increase of diffusivity for $\Delta\gg\tau_c$ and, in general, much lower values of the mean-squared particle displacements. Investigations of the mixing process of dye particles with artificially reduced cohesivity [14], on the other hand, seem to corroborate our results as they indicate a relatively broad region of fluid-like behavior below the onset of bubbling in which particles are mobile.

It is interesting to note that for the smaller catalyst particles, the transition is less smooth and that the fast diffusion component dominates for all but the lowest air velocities [see Figs. 2(b) and 2(c)]. This might be a consequence of the fact that the regime prior to the transition to the bubbling phase is less well covered. A particular feature is found for particles

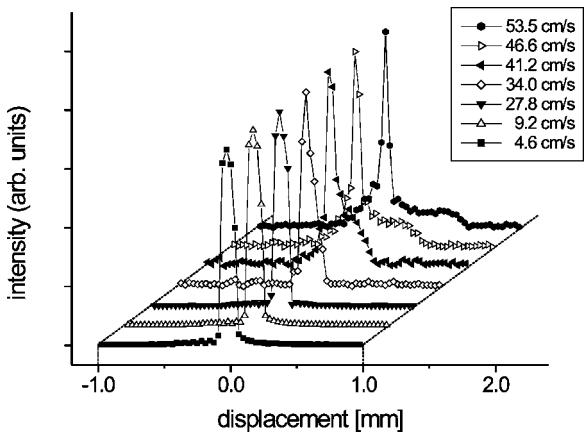


FIG. 4. Particle displacement statistics (propagators) for poppy seeds at different air flow velocities. All propagators are normalized to equal maximum peak height.

with diameters 112–140 $\mu$m where for the lowest flow rate ($v=0.34$ cm/s), $\tilde{S}(q,\Delta)$ decays to one half its initial density and then remains constant for the whole range of gradients applied, suggesting a much less mobile fraction of particles in the bed [see Fig. 2(c)]. In no case can a pronounced peak at a particular wave number be observed, as would be expected in the analogous case of restricted diffusion within a well-defined confined geometry [12,13].

The crossovers between different regimes as obtained from density and diffusion measurements coincide with each other reasonably well. By comparison of Figs. 1(b) and 3, one can assign the onset of the bubbling phase to the beginning of the plateau in the bed density and to the beginning of a pronounced increase of the effective diffusivity, both occurring around $v=12$ m/s for the largest catalyst particles and being shifted towards lower-gas velocities for smaller particles.

The probability densities of displacements along the gravity axis, $\bar{P}(Z)$, reflect the observation of a bicomponent decay shape present in the $q$-data picture. In Fig. 4, the propagators obtained for poppy seeds at different air flow rates are compared to each other; experimental parameters have been $\delta=0.5$ ms and $\Delta=2.1$ ms for these experiments. Very similar results were found for the catalyst samples.

A narrow peak represents particles with small displacements (see Fig. 4), while a second fraction of particles is found to have considerably larger displacements. Note that for the relatively short encoding times $\Delta$ used in this study, displacements larger than about one-particle diameter are not found, suggesting that even for the much-reduced bed density, an exchange of particles over distances much exceeding the local cage size is still unlikely to happen for the given ratio $\Delta/\tau_c$. A clearly asymmetric propagator is observed for poppy seeds at high gas velocities above the transition to a bubbling phase. A possible explanation might be a scenario where some particles are carried along rising gas bubbles with a reduced probability of collisions and, as a consequence, a higher effective velocity; the collision rate becomes increased again for falling particles, resulting in a smaller maximum negative velocity along the direction of gas flow.

In conclusion, we have shown the feasibility of obtaining direction-dependent particle displacement distribution functions as well as average quantities such as mean diffusivity and bed density in a gas-fluidized bed of particles by means of NMR ***k***-space and ***q***-space imaging techniques. Crossovers representing the granular-media equivalents to phase transitions in condensed matter could be verified by different techniques independently. The propagators of displacements were found to be distinctly asymmetric with much larger maximum velocities occurring along the direction of the gas pressure gradient. The noninvasive character of NMR and its ability to combine informations such as chemical composition, position, and velocity by employing suitable techniques has the potential to investigate a wide variety of granular motion phenomena, provided that signal encoding is made feasible by a sufficient amount of liquid matter in the granular particles. The continuation of such investigations will involve the separate determination of displacement statistics in different spatial directions, at different encoding times and the measurement of higher-order correlations in particle motions being supplemented by numerical simulations of the particle motion characteristics.

Financial support from the Deutsche Forschungsgemeinschaft DFG (Bl 231/25-1) is gratefully acknowledged.

[1] *Fluidization*, edited by J. F. Davidson, R. Clift, and D. Harrison (Academic, London, 1985).
[2] *Gas Fluidization Technology*, edited by D. Geldart (Wiley-Interscience, New York, 1986).
[3] K. Ichiki and H. Hayakawa, Phys. Rev. E **52**, 658 (1995).
[4] K. Ichiki and H. Hayakawa, Phys. Rev. E **57**, 1990 (1998).
[5] N. Menon and D. J. Durian, Science **275**, 1920 (1997).
[6] N. Menon and D. J. Durian, Phys. Rev. Lett. **79**, 3407 (1997).
[7] P. T. Callaghan, *Principles of Nuclear Magnetic Resonance Microscopy* (Clarendon Press, Oxford, 1991).
[8] B. Blümich, *NMR Imaging of Materials* (Clarendon Press, Oxford, 2000).
[9] A. Caprihan and J. D. Seymour, J. Magn. Reson. **144**, 96 (2000).
[10] X. Yang and D. Candela, Phys. Rev. Lett. **85**, 298 (2000).
[11] P. T. Callaghan and J. Stepišnik, Adv. Magn. Opt. Reson. **19**, 325 (1996).
[12] P. T. Callaghan, A. Coy, D. MacGowan, K. J. Packer, and F. O. Zelaya, Nature (London) **351**, 467 (1991).
[13] P. T. Callaghan, A. Coy, T. P. J. Halpin, D. MacGowan, K. J. Packer, and F. O. Zelaya, J. Chem. Phys. **97**, 651 (1992).
[14] J. M. Valverde, A. Castellanos, and M. A. S. Quintanilla, Phys. Rev. Lett. **86**, 3020 (2001).